Effective Control of the Ratio of Red to Green Emission in Upconverting LaF_3 Nanoparticles Codoped with Yb^{3+} and Ho^{3+} Ions Embedded in a Silica Matrix

Jothirmayanantham Pichaandi,[†] Frank C. J. M. van Veggel,*[,†] and Mati Raudsepp[‡]

Department of Chemistry, University of Victoria, P.O. Box 3065, Victoria, British Columbia, Canada V8W 3V6, and Department of Earth and Ocean Sciences, The University of British Columbia, Vancouver, British Columbia, Canada V6T 1Z4

ABSTRACT The red to green ratio from upconversion in Yb^{3+} and Ho^{3+} codoped LaF_3 nanoparticles embedded in a silica matrix can be controlled by careful tuning of the sol−gel process. Red to green ratios of 1:2.3 to 23:1 were observed from the samples that had the same composition of Yb^{3+} and Ho^{3+} ions codoped LaF_3 nanoparticles. The varied ratios were achieved by changing the aging and drying time of the sol−gel and the subsequent annealing process at elevated temperatures. XRD measurements showed that the sample that gave a red to green ratio of 23:1 had large amounts of amorphous silica, whereas the sample that gave a ratio of 1:2.3 had cristobalite, i.e., crystalline silica, in excess. The phonon energy of amorphous silica is higher than that of cristobalite, so quenching of the green emission effectively resulted in enhanced red emission. To prove that amorphous silica has a higher phonon energy, we completed upconversion luminescence studies at 77 K, which resulted in a decrease in the red to green ratio by a factor of 3. This indeed proves that the phonon energy of amorphous silica is the factor for observing enhanced red emission and a good control over the ratio of red to green. Infrared spectra show Si−O stretching vibrations over a broader energy range for amorphous silica than cristobalite which thus more easily matches with the difference in the energy levels of Ho^{3+} ions, making the quenching process more efficient. To substantiate the above evidence, we performed partial etching of samples where enhanced red to green ratio was observed, and XRD results show the presence of amorphous silica and LaF_3 nanoparticles. After nearly complete etching of the silica, XRD results show the presence of LaF_3 and very little silica.

KEYWORDS: nanoparticles • LaF_3 • upconversion • lanthanide • holmium • ytterbium • silica matrix

INTRODUCTION

Upconversion is a process that converts two or more lower-energy photons into one higher-energy photon. Most of the upconversion processes in the case of lanthanide ions are stepwise two-photon processes (1−3). However, there are some exceptions, like photon avalanche processes (1, 4) and the stepwise three-photon (5−10) process for upconverted blue light from Tm^{3+} ions. One such interesting photon avalanche type of process is the hetero-LEET mechanism, which has been reported by our group (11). Up-conversion through lanthanide nanoparticles has been studied extensively in various matrices especially with Yb^{3+} and Er^{3+} ions (12−22). Several matrices like LaF_3, $NaYF_4$, Y_2O_3, KYF_4, YVO_4, and nanoparticles codoped with Yb^{3+} and Er^{3+} ions have been synthesized and studied in detail. A lot of effort has gone into synthesizing new materials for doping with Yb^{3+} and Er^{3+}. These nanoparticles are regarded as interesting materials for application in biolabels, LEDs, security labels, monitoring, drug delivery, etc. (7, 19, 23−30). Generally, Yb^{3+} and Er^{3+} codoped systems give a bright green emission along with a weak red emission. On the other hand, Zhao et al. (31) reported enhanced red emission in $NaYF_4$ nanoparticles codoped with Yb^{3+} and Er^{3+} ions. They observed that the presence of citrate ligands and OH groups from the hydrothermal synthesis result in the quenching of green emission and enhancement of red emission. In addition, Li et al. (32) argue that very high Yb^{3+} doping and calcination of Gd_2O_3 at lower temperatures result in enhanced red emission. Even though Yb^{3+} and Ho^{3+} codoped nanoparticles are similar to Yb^{3+} and Er^{3+} systems in terms of upconversion properties, only a handful of papers deal with these nanomaterials (33−36). These papers have studied the upconversion properties by changing the concentration of Yb^{3+} and Ho^{3+} ions in the nanoparticles. Typically, the upconversion through Yb^{3+} and Ho^{3+} codoped systems result in an intense green emission accompanied by a weak red emission. However, there are only a few reports on enhanced red emission from Yb^{3+} and Ho^{3+} codoped upconversion process. The enhanced red emission observed by Yi et al. (37) in LaF_3 nanoparticles codoped with Yb^{3+} and Ho^{3+} ions has been attributed to the presence of organic ligands stabilizing the particles that quench the green emission. Lisiecki et al. (38) have reported that high doping levels of Yb^{3+} ions and high phonon energy of YVO_4 nano-

* Corresponding author. E-mail: fvv@uvic.ca.
Received for review September 16, 2009 and accepted December 11, 2009
[†] University of Victoria.
[‡] The University of British Columbia.
DOI: 10.1021/am900630c

Table 1. Change in Red (R) to Green (G) Ratio As a Function of Aging and Drying Time of $La_{0.76}Yb_{0.22}Ho_{0.02}F_3$ Embedded in a Silica Matrix[a]

		drying time		baking time				
sample	aging time (days)	78 °C	92 °C	300 °C	400 °C	500 °C	800 °C	red:green ratio
1	2	45 min	0 min	0 min	30 min	0	12 h	1:2.3
2	3	2 h	0 min	0 min	30 min	0	12 h	1:1.5
3	4	2 h 30 min	0 min	0 min	30 min	0	12 h	1:1
4	4	2 h	2 h	0 min	30 min	0	12 h	3.2:1
5	6	2 h	4 h	4 h	0 min	4 h	12 h	6.3:1
6	15	2 h	11 h	8 h	0 min	8 h	12 h	23:1

[a] All ramping procedures for samples are the same as detailed in the Experimental Section.

particles facilitate the enhancement of red emission. Our group has also reported that when LaF_3 nanoparticles were codoped with high levels of Yb^{3+} and Ho^{3+} ions and then coated with silica they got converted to lanthanum silicate which has phonon energy of 1200 cm^{-1}. So because of its higher phonon energy than LaF_3, the lanthanum silicate matrix quenches the $^5I_6$ level populating the $^5I_7$ level of Ho^{3+} ions (39). This results in more and more photons reaching the $^5F_5$ level from the $^5I_7$ level, which subsequently emits red light. This results in an increased red emission when compared to green emission. However, there are no reports on how to control the ratio of visible emissions from upconversion. Controlling the emission in upconversion process will help in tuning the color of the light, which will be very useful for constructing, for example, an upconversion laser with near-infrared excitation. In this paper, we report the effective control of red to green ratio in an upconversion process involving Yb^{3+} and Ho^{3+} ions codoped in LaF_3 nanoparticles that are embedded in a silica matrix. LaF_3 was chosen as the matrix to be codoped with Yb^{3+} and Ho^{3+} because of its low phonon energy (300 cm^{-1}) (40). There are two reasons for embedding lanthanide nanoparticles in a silica matrix using sol−gel technique. The first reason is that the as-synthesized nanoparticles do not show any emission due to upconversion. They have to be baked to remove OH groups and organic ligands, which would quench all the energy levels involved in the upconversion process resulting in no emission. Baking would convert the nanoparticles into the bulk form of the material and render them not suitable for further modifications. To overcome this problem, we embedded the nanoparticles in a silica matrix using sol−gel technique, which makes the material a potential candidate for applications like integrated optics, planar waveguides, upconversion lasers, and fiber amplifiers (4, 41−43). The second reason is that silica also prevents the nanoparticles from aggregation and improves the luminescent properties of the nanoparticles when compared to the doping of lanthanide ions directly in silica (44). An increase in the red emission is normally attributed to the high amount of Yb^{3+} doping in the sample which results in increased energy transfer from Yb^{3+} ions to Ho^{3+} ions as well as the back transfer of energy from $^5S_2$ level of Ho^{3+} ions to $^2F_{5/2}$ of Yb^{3+} resulting in quenching of green emission. In this report, we show that a high Yb^{3+} concentration in our nanoparticles is not responsible for the control of red to green ratio and prove that the ratio is controlled by the amount of cristobalite (crystalline silica) and amorphous silica present in the sample after baking of the sol−gel.

EXPERIMENTAL SECTION

Chemicals. All chemicals were obtained from Sigma-Aldrich and were used as such without any further purification. Lanthanide nitrate salts used were of the highest possible purity of 99.9%. An aqueous solution of ammonium hydroxide was used that had a concentration of 28.0 to 30.0 wt %. HF (48−51%) was bought from ACF Chemicals.

Synthesis of LaF_3 Particles Codoped with Yb^{3+} and Ho^{3+}. The synthesis of LaF_3 nanoparticles codoped with Yb^{3+} and Ho^{3+} was adapted from the procedure published by our research group (30). Citric acid (2 g) was mixed with 35 mL of distilled water, which was purged with argon was heated to 75 °C. Ammonia (1.2 mL) was added to bring the pH to between 5.5 and 6. To this solution was added dropwise 1.33 mmol of lanthanide nitrate ($La_{(1-x-y)}$, Yb_x, Ho_y) salts dissolved in 2 mL of methanol to the above solution. Following this, 3 mmol of NaF in 2 mL of distilled water was added dropwise. The reaction was continued for 2 h and the solution was then cooled to room temperature. Ethanol (40 mL) was used to precipitate the nanoparticles and they were collected by centrifuging at 4500 rpm for 5 min to separate the particles. The particles were dried in air overnight to obtain a white powder, which was completely dispersible in water. Nanoparticles with varying doping levels of Yb^{3+} ions were synthesized keeping the Ho^{3+} doping level constant at 5 mol %.

Silica Sol−Gel Containing LaF_3 Nanoparticles Codoped with Yb^{3+} and Ho^{3+} ions. Silica sol−gel containing LaF_3 nanoparticles codoped with Yb^{3+} and Ho^{3+} ions was synthesized by adapting the procedure of Sivakumar et al. (30) Tetraethyl orthosilicate (TEOS) (2 mL) was mixed with 8 mL of ethanol to which 50 to 60 mg of the LaF_3 nanoparticles codoped with Yb^{3+} and Ho^{3+} ions dissolved in 2 mL of distilled water was added. HCl of 0.1 M concentration was added in drops to bring the pH between 0 and 1. The sols were then aged for a minimum of 2 to a maximum of 15 days.

Two representative procedures will be described here and the details for all samples are presented in Table 1. The sol−gel sample (1) was aged for 2 days and then dried in a rotary evaporator under a vacuum (using an aspirator) for 45 min at 78 °C to get a white powder. The sol−gel powder was then baked in a furnace with the following procedure. The sample was heated at the rate of 4°/min to reach 400 °C and kept at that temperature for 30 min. The sample was then heated to 800 °C at the rate of 3.33 deg/min, and maintained at that temperature for 12 h. The sol−gel sample (6) aged for 15 days was dried in a rotary evaporator under a vacuum at 78 °C for 2 h. Following this, the temperature was increased to 92 °C and kept at that temperature for 11 h. The dried sol−gel was baked

with the following procedure. The sample was heated to 300 °C at a rate of 3.33°/min and maintained at that temperature for 8 h. The temperature was then increased to 500 °C at 6.66°/min and kept constant at that temperature for 8 h. Eventually, the sol−gel powder was heated to 800 °C at the rate of 2.5°/min and baked at that temperature for 12 h.

HF Etching of the Particles. Approximately 225 mg of LaF_3 nanoparticles embedded in the silica matrix were mixed with 36 mL of 2% HF and etched for 3 h. The particles were centrifuged at 13 500 rpm for 20 min which were then washed with 25 mL of water to remove HF. It was observed that 110 mg of particles was obtained after this etching step. The particles obtained from the above etching process were subjected to the same process again. The amount of particles obtained was around 15−20 mg.

X-ray Diffraction (XRD) Measurements. XRD patterns in Figures 3−5 and Figure S8 in the Supporting Information were measured using the following procedure. Step scan X-ray powder diffraction data were collected over a 2θ range of 3−80° on a Siemens D5000 Bragg−Brentano θ-2θ diffractometer equipped with a Fe monochromator foil, 0.6 mm (0.3°) divergence slit, incident- and diffracted-beam Soller slits, and a VÅNTEC-1 strip detector. Co X-ray tube was operated at 35 KV and 40 mA using a takeoff angle of 6°. The scanning step size is 0.04° 2θ with a counting time of 1 s per step. Rietveld refinements were done using the program Topas 3.1 (Bruker-AXS).

Patterns in Figures S6 and S9 in the Supporting Information were measured with Cr (30 kV, 15 mA) radiation on a Rigaku Miniflex diffractometer using a zero-background holder with variable divergence slit, 4.2° scattering slit, and 0.3 mm receiving slit. The scanning step size is 0.02° 2θ with a counting time of 6 s per step over the 2θ range of 20−140°.

The amount of sample was 40−50 mg, which was ground in an alumina mortar to break up the lumps.

Fluorescence Measurements. Upconversion experiments were carried out with an Edinburgh Instruments FLS920 fluorimeter with the sample being excited with a 980 nm JDS Uniphase laser diode (device- 63−0042) which was coupled to a 105 μm core fiber. To collimate the output of the 980 nm diode laser a Newport F-91-C1-T Multimode Fiber Coupler was used and an 850 nm long band-pass filter was used to block some spurious emissions from the diode laser. The emission was collected using a red-sensitive Peltier-cooled Hamamatsu R955 PMT. The scattered light from the diode laser was removed using an 800 nm short band-pass filter. The samples were held in a quartz EPR tube. For low-temperature measurements, the samples were held in a liquid nitrogen-cooled EPR dewar. The samples were excited with a power density of 80 W/cm^2. There was no visible change in the upconversion spectra or any change in the ratio of red to green because of the sample getting heated by the laser power. The ratio of red to green was calculated using the integrated intensity of the respective peaks. All the spectra were corrected for the instrument response.

Energy-Dispersive X-ray Spectroscopy (EDS). EDS was done using a Hitachi S-3500N scanning electron microscope, operated at 20 kV and a resolution of 102 eV. Dry powdered samples were tagged on to the substrate using a double-sided carbon tape and mounted onto the sample holder. Three measurements were done for each sample to calculate standard deviations.

Infrared (IR) Spectroscopy. The IR spectrum was measured using an IR200 spectrometer from Thermo Instruments (Canada) Inc. Four scans were done for reference and the sample with a resolution of 2 cm^{-1}. Air was used as the reference for the measurement.

RESULTS AND DISCUSSION

Size and EDS Measurements. The LaF_3 nanoparticles codoped with Yb^{3+} and Ho^{3+} ions were synthesized using methods very similar to previously published protocols (30, 44−46) and their size was found to be 5−7 nm from XRD measurements using the Scherrer equation. The doping level in nanoparticles is often expected to be the same as added in the reaction mixture, but this is not necessarily the case. Energy-dispersive X-ray spectroscopy (EDS) results show that nominal doping levels of 50, 40, 30, and 10 at % Yb^{3+} ions in the reaction resulted in 22, 17, 12, and 4 at %, respectively, in the LaF_3 nanoparticles. A reaction mixture with 5 at % of Ho^{3+} ions resulted in 2 at % in the final product. A representative spectrum is shown in Figure S1 in the Supporting Information.

Influence of Aging Drying and Baking on Luminescent Properties. The ratio of red to green (Figure 1A) could be controlled from 1:2.3 to 23:1 by changing the parameters like aging time, drying time, and baking pattern of the silica sol−gel. All three parameters had to be changed in order to get the desired ratio, so the overall effect is highly convoluted. Sample 1 (Table 1), which was aged for 2 days and dried in rotary evaporator for 45 min and baked at 800 °C, gave a strong green emission when compared to red emission as shown in Figure 1, in which the red to green ratio is 1:2.3. The green (540 nm), red (654 nm) and 750 nm emissions correspond to $^5S_2$ to $^5I_8$, $^5F_5$ to $^5I_8$, and $^5S_2$ to $^5I_7$ transitions of Ho^{3+}, respectively (Figure 1A, 1B). When Ho^{3+} was excited at 450 nm, we observed a green and 750 nm emission along with a very weak red emission (see Figure S2A in the Supporting Information). This proves that green does not feed the red emission. To confirm whether the $^5S_2$ energy level is responsible for the 750 nm emission, we excited the sample at 540 nm, for which indeed a peak at 750 nm was observed (see Figure S2B in the Supporting Information). The absence of red emission is further confirmation that the $^5S_2$ level is responsible for 750 nm emission. With the help of this evidence and the report from Boyer et al. (34), a probable mechanism is proposed (Figure 1B). A very detailed study of the proposed mechanism is currently being done and will be reported in a separate publication. A strong green emission in comparison with a weak red emission was observed for a similar sample like sample 1 when it was aged for 15 days and dried for 45 min in a rotary evaporator. When a sample was aged for 2 days and dried in a rotary evaporator for 5 h, the ratio of red to green was still 2.3 to 1. As the aging time was varied from 2 to 15 days combined with a gradual increase in drying time of the sol, a progressive increase in the ratio of red to green was seen (Figure 1A). The maximum ratio of 23:1 was obtained for sample 6, which was aged for 15 days and dried for 11 h before annealing. This implied that drying plays a vital role in controlling the ratio. An interesting factor to note is that all ratios were observed for the same composition, i.e., $La_{0.76}Yb_{0.22}Ho_{0.02}F_3$ nanoparticles embedded in a silica matrix. Baking also proved to be an important factor in observing enhanced red emission. The samples 1−4 were

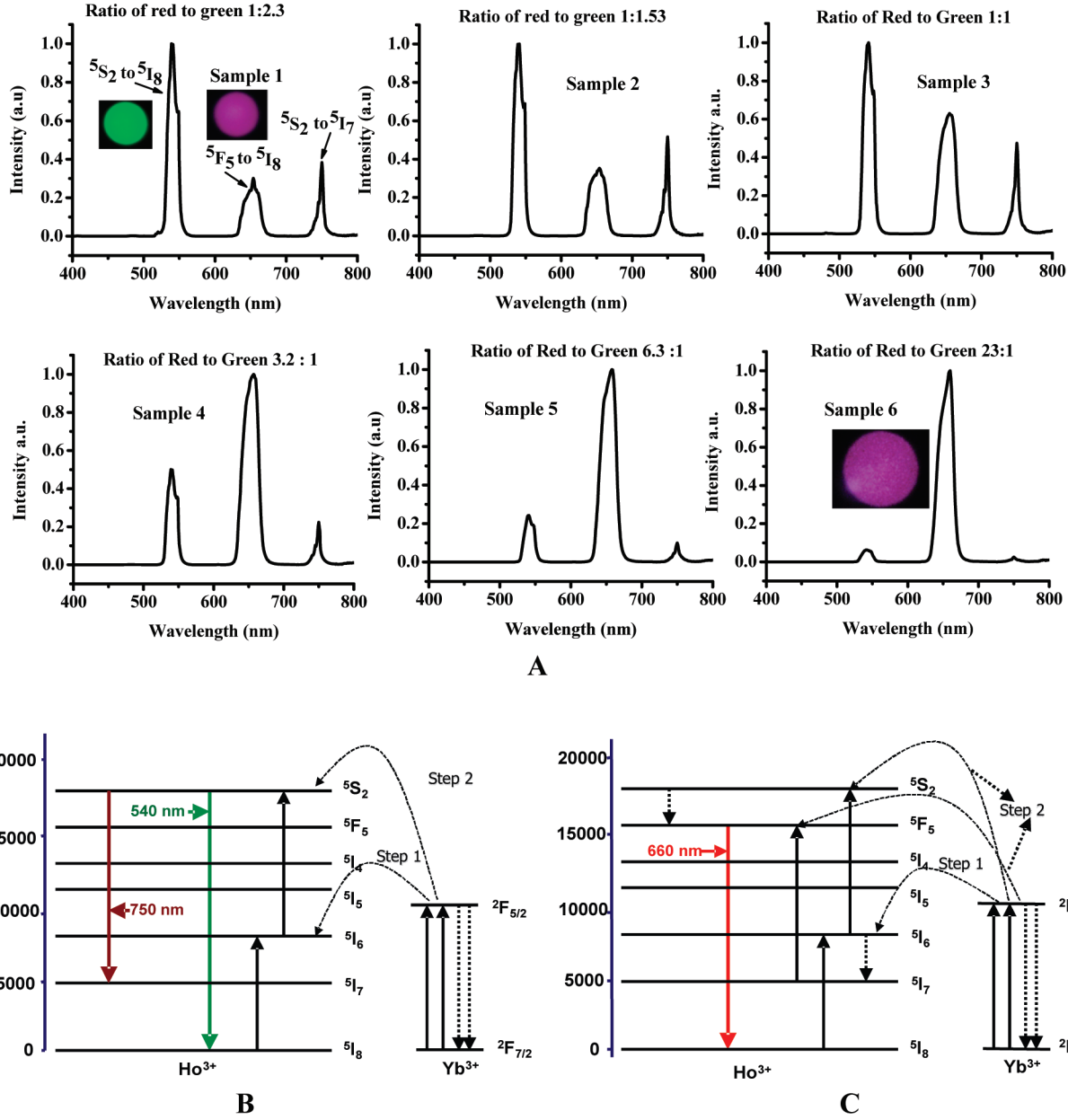

FIGURE 1. (A) Different red to green ratio seen in upconversion luminescence from samples of the same composition ($La_{0.76}Yb_{0.22}Ho_{0.02}F_3$ embedded in a silica matrix). Insets: red light pictures in sample 1 and 6 were photographed using a 590 nm filter and no filter was used for green light in sample 1. (B) Probable mechanism for green emission (peak at 540 nm) and 750 nm emission. (C) Probable mechanism for red emission (peak at 654 nm).

baked at 800 °C for 12 h, whereas samples 5 and 6 were baked at 300 and 500 °C before baking at 800 °C for 12 h. For samples 5 and 6 baking at 300 and 500 °C was necessary along with the increase in aging and drying time to see an enhanced red emission. This proves that all the three parameters aging, drying, and baking plays an important role in controlling the ratio of red to green. This trend of high red to green ratio was seen for other doping levels of Yb^{3+} ions. The red to green ratio for 17% Yb^{3+} codoped nanoparticles embedded in a silica matrix obtained was 42:1 (Figure 2C). In the case of 12 and 4 atom percent doping with Yb^{3+} ions the red to green ratio was 18:1 and 23:1 respectively (Figure 2A,B). The varied red to green ratios was also observed for 12 mol percent Yb^{3+} concentrations (see Figure S3 in the Supporting Information). As expected, we also observed that with an increase in the amount of Yb^{3+} concentrations in the nanoparticles the amount of red and green also increased which can be seen from Figure S4 in the Supporting Information. The power dependence curves (see Figure S5 in the Supporting Information) show that both green and red emissions are two-photon processes, and the ratios of red to green at various power densities remain the same. The slope over the first seven points is between 1.9 and 2.0, with a slight decrease in the slope to 1.6 to 1.7 at higher power densities because of saturation effects. The ratio of green to 750 nm emission changes for samples 1−6, which can be attributed to the change in the branching ratios of $^5S_2$ to $^5I_8$ and $^5I_7$ because of the subtle difference in the coordination sphere of the surface Ho^{3+} ions because of differences in amorphous silica and cristobalite. There is

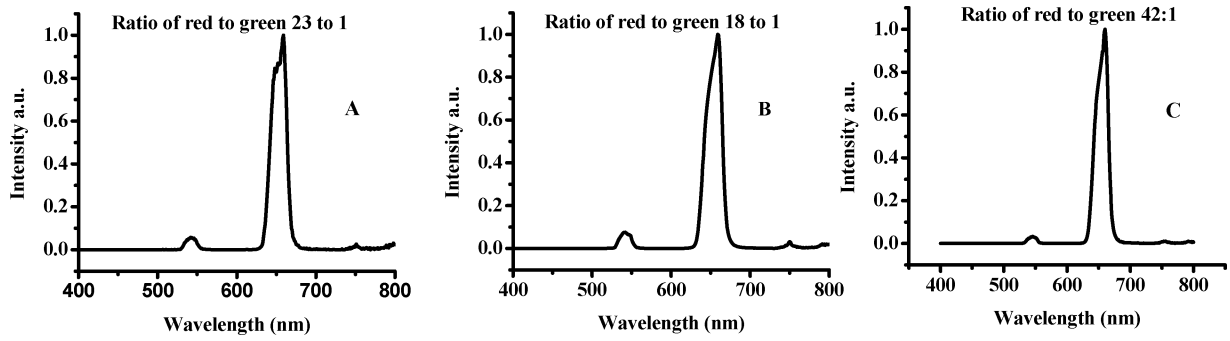

FIGURE 2. Different red to green ratio seen in upconversion luminescence from samples of the different composition (A) $La_{0.94}Yb_{0.04}Ho_{0.02}F_3$, (B) $La_{0.86}Yb_{0.12}Ho_{0.02}F_3$, (C) $La_{0.81}b_{0.17}Ho_{0.02}F_3$. All samples were embedded in a silica matrix.

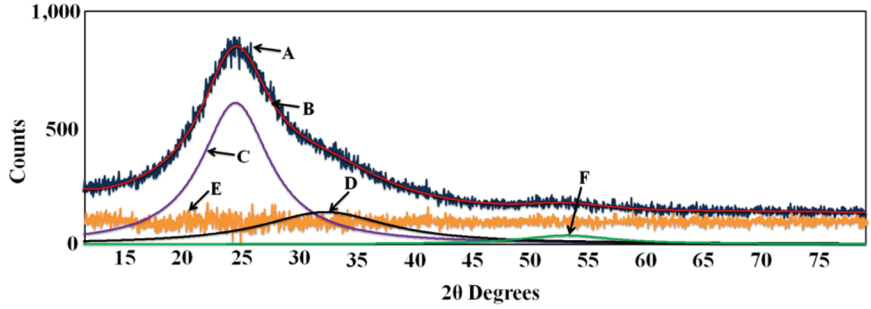

FIGURE 3. XRD pattern of baked $La_{0.76}Yb_{0.22}Ho_{0.02}F_3$ nanoparticles embedded in a silica matrix (enhanced red emission); 23:1 red to green ratio: (A) observed pattern, (B) calculated pattern, (C, D, F) from peaks fitted to amorphous silica, (E) residual curve.

precedent for this effect based on Eu^{3+}-doped LaF_3 nanoparticles that are embedded in the silica matrix (44).

XRD Measurements and Etching with HF. Some of our previous reports initially suggested that the high red to green ratio obtained might be due to the fact that LaF_3 could have be converted to lanthanum silicate (44), which has a higher phonon energy than LaF_3. However, XRD results did not suggest the presence of lanthanum silicate for samples showing high red to green ratios. Instead, the XRD results indicated that sample 6 (Figure 3) had amorphous silica and no apparent traces of any other compound. This can be attributed to the fact that the presence of large amounts of amorphous silica masks the signal from LaF_3 and potentially others compounds. This is because the amount of LaF_3 in the sol is around ~7.5 wt %, which is not very high when compared to that of amorphous silica. To find out whether LaF_3 was present along with amorphous silica, we completely etched the sample with 2% HF. XRD results proved that the compound had LaF_3 (see Figure S6 in the Supporting Information) and not lanthanum silicate (44). The reason why lanthanum silicate was not formed is because of the fact that the sol was dried in a rotary evaporator for a very long time, which would have converted $Si(OH)_4$ in the sol to SiO_2. For lanthanum silicate to have formed, $Si(OH)_4$ has to react with LaF_3 at elevated temperatures to remove the fluoride as HF. The formation of amorphous silica can be attributed to the drying process in a vacuum in a rotary evaporator for long hours and annealing at 500 and 800 °C for several hours. Moreover, the XRD results for sample 1 in Figure 4 (low red to green ratio) show a large amount of cristobalite along with amorphous silica and LaF_3. If the difference in XRD is just the amount of amorphous silica between sample 6 and 1, the plausible explanation for getting enhanced red to green ratio is that the phonon energy of amorphous silica has to be higher than that of cristobalite. One way to confirm that amorphous silica is responsible for the enhanced red to green ratio sample 6 was partially etched with 2% HF. The partially etched sample still gave an enhanced red emission with reduction in ratio of red to green from 23:1 to 12:1 (see Figure S7 in the Supporting Information). XRD results show that the partially etched samples had LaF_3, a large hump for amorphous silica, and a sharp peak for cristobalite (Figure 5). Amorphous silica etches faster when compared to crystalline silica (47), which corroborates our results where cristobalite and LaF_3 are observed after partial etching. The reason why cristobalite was not observed before etching might be due to the fact that the presence of large amounts of amorphous silica has masked the signal from cristobalite. The reduction in the red to green ratio after partial etching and a diminished red to green ratio for samples with large amounts of cristobalite proves that the ratio of cristobalite to amorphous silica is decisive for the ratio of red to green. If cristobalite is present in large amounts when compared to amorphous silica, a decrease in the red to green ratio is observed, whereas for amorphous silica, a big augmentation in the red to green ratio is observed. This is further substantiated by the fact that sample 1 had large amounts of cristobalite along with LaF_3 and amorphous silica, whereas sample D ($La_{0.86}Yb_{0.12}Ho_{0.02}F_3$, see Figure S8 in the Supporting Information) had large amounts of amorphous silica along with cristobalite and LaF_3. Excess amorphous silica can be seen from XRD which shows a broader peak for silica in sample D when compared to sample 1 referring to large amounts of amorphous silica. When sample 6 was completely etched a strong green was observed when compared to a weak red

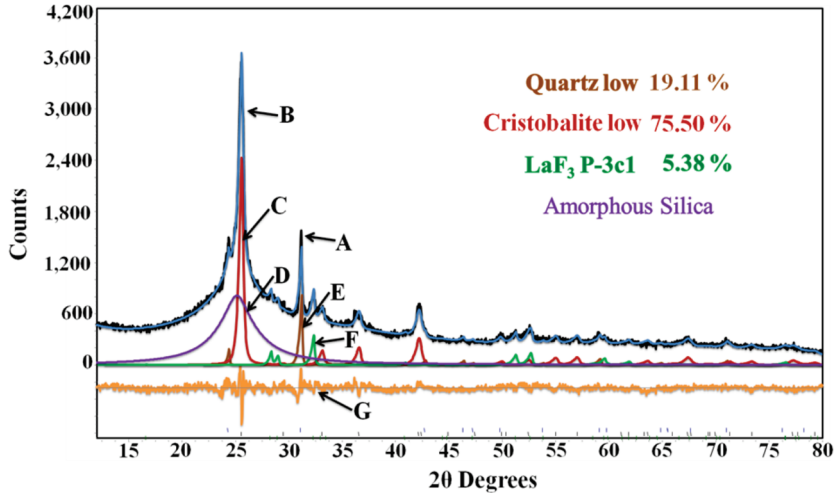

FIGURE 4. Rietveld refinement plot of baked $La_{0.76}Yb_{0.22}Ho_{0.02}F_3$ nanoparticles embedded in a silica matrix (enhanced green emission) 1:2.3 red to green ratio sample: (A) observed pattern, (B) calculated pattern, (C) cristobalite, (D) amorphous silica, (E) quartz low, (F) LaF_3 $P3\bar{c}1$, (G) residual curve. The weight percent does not include amorphous silica.

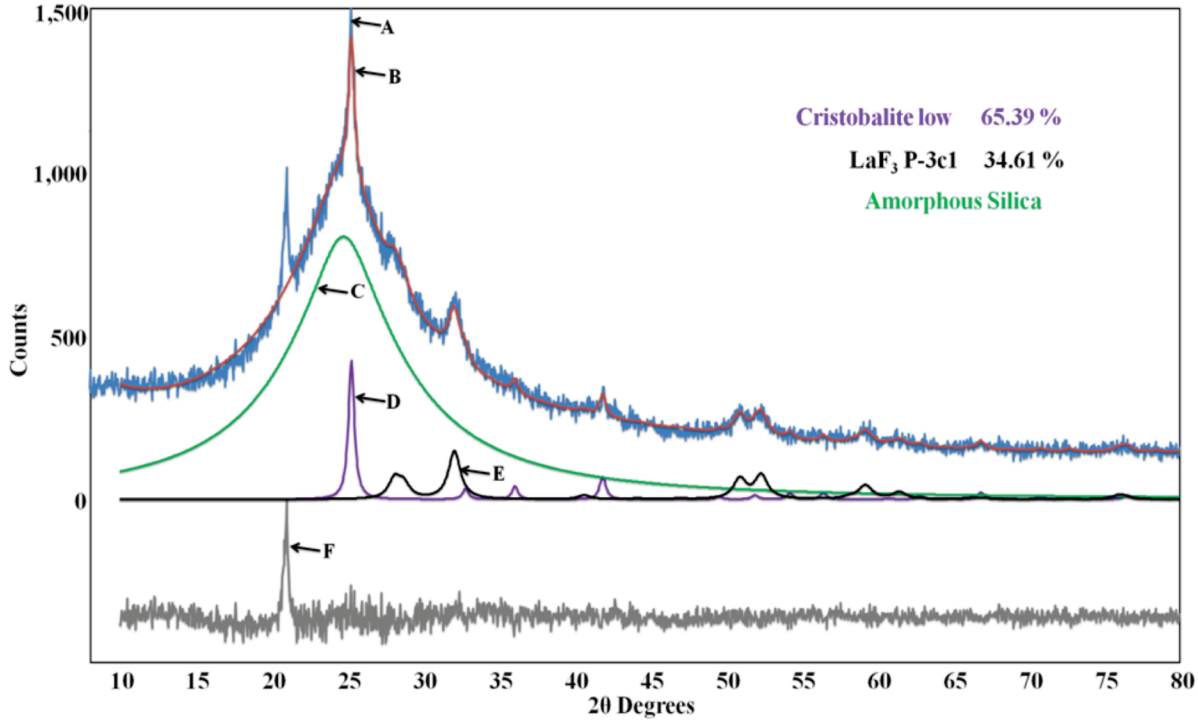

FIGURE 5. Rietveld refinement plot of partially etched $La_{0.76}Yb_{0.22}Ho_{0.02}F_3$ nanoparticles embedded in a silica matrix: (A) observed pattern, (B) calculated pattern, (C) amorphous silica, (D) cristobalite, (E) $LaF_3P3\bar{c}1$, (F) residual peak. The weight percent does not include amorphous silica.

emission resulting in a much diminished red to green ratio of 1:2.3. This proves that amorphous silica is responsible for enhancing the red to green ratio. Sample 1 was also completely etched to remove cristobalite to see whether there is a further decrease in the ratio of red to green from 1:2.3. The etched sample showed the same red to green ratio as before and XRD results showed that LaF_3 was present, which can be seen in Figure S9 in the Supporting Information. This might be due to the fact that the XRD shows the presence of small amounts of silica still attached to the LaF_3 nanoparticles even after nearly complete etching and the presence of water on the surface of the nanoparticles. Both quench the green emission, probably resulting in the same red to green ratio as seen before etching.

Low-Temperature Upconversion Measurements at 77 K. Another way to prove that the differences in the phonon energy are responsible for the enhanced red emission is to measure the upconversion spectrum at 77 K. What we expected at low temperatures was that red emission would subside to a very good extent and we would see a significant change in the ratio of red to green. These measurements showed that the ratio of red to green for $La_{0.86}Yb_{0.12}Ho_{0.02}F_3$ nanoparticles embedded in a silica matrix indeed decreased from 18:1 to 5.8:1, as seen in Figure

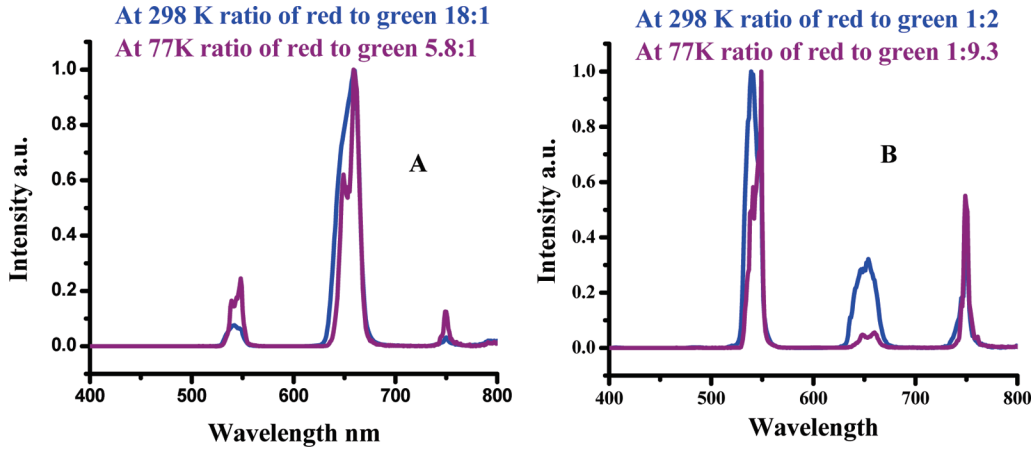

FIGURE 6. Upconversion spectra of $La_{0.86}Yb_{0.12}Ho_{0.02}$ nanoparticles embedded in a silica matrix at 298 and 77 K: (A) sample aged for 15 days, (B) sample aged for 2 days.

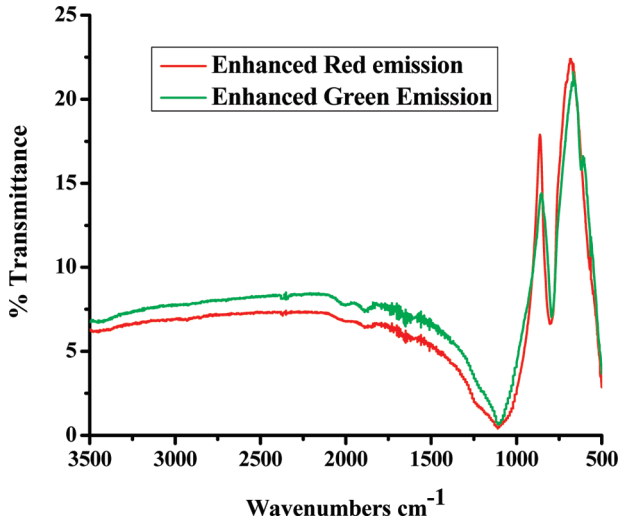

FIGURE 7. IR spectra for $La_{0.76}Yb_{0.22}Ho_{0.02}F_3$ nanoparticles embedded in a silica matrix (enhanced green emission and enhanced red emission). Enhanced green emission transmittance values were decreased by a factor of 1.5 in order to make an easy comparison with the enhanced red emission values.

6A. When the low-temperature measurements were carried out for the sample $La_{0.86}Yb_{0.12}Ho_{0.02}F_3$ (Figure 6B), we observed enhanced green and the ratio changed from 1:2.3 to 1:9. This proves that the phonon energy at room temperature plays a very important role in the amount of red that is observed and the control over the ratio of red to green. A slight shift in the peaks to higher wavelength, i.e., lower energy (Figure 6), is observed for the low-temperature spectra, as expected based on the Boltzmann distribution.

Infrared (IR) Spectra. The third piece of evidence that supports this explanation was obtained for the IR spectra of the samples 1 and 6, which gave enhanced green and enhanced red, respectively. Both samples showed peaks at 1100 cm^{-1} corresponding to the Si−O−Si stretch. The sample giving enhanced red showed a broad peak at 1100 cm^{-1} when compared to the sample that shows a dominant green emission (Figure 7). So amorphous silica has a higher number of lower and higher energy phonons when compared to cristobalite. Because of the broader phonon energy distribution of amorphous silica, the difference in the energy levels of Ho^{3+} ions can more easily be matched with a number of higher and lower energy phonons. This makes the quenching process more efficient for amorphous silica than cristobalite.

CONCLUSIONS

We observed that a simple change in the experimental conditions resulted in the enhancement of red emission and the excellent control over red to green ratio in the upconversion process from Yb^{3+} and Ho^{3+} ions codoped LaF_3 nanoparticles in a silica matrix. IR spectra, upconversion at 77 K, and HF etching provided concrete evidence that the ratio of amorphous to crystalline silica is responsible for such big variations in the upconversion properties of these samples. A series of ratios for red to green from 1:2.3 to 23:1 was obtained. The interesting factor is that the ratios could be controlled in a single Yb^{3+} and Ho^{3+} doping composition.

Acknowledgment. The Canada Foundation for Innnovation (CFI), The British Columbia Knowledge Development Fund (BCKDF), and Natural Science and Engineering Council of Canada (NSERC) are gratefully acknowledged for their financial support.

Supporting Information Available: EDS spectra (Figure S1), upconversion luminescence spectra (Figures S2−S4, S7), power dependence curves (Figure S5), and XRD spectra (Figures S6, S8, S9) (PDF). This material is available free of charge via the Internet at http://pubs.acs.org.

REFERENCES AND NOTES

(1) Auzel, F. *Chem. Rev.* **2004**, *104*, 139.
(2) Auzel, F.; Pecile, D. *J. Lumin.* **1973**, *8*, 32.
(3) Wang, F.; Liu, X. G. *Chem. Soc. Rev.* **2009**, *38*, 976.
(4) Joubert, M. F. *Opt. Mater.* **1999**, *11*, 181.
(5) Boyer, J. C.; Vetrone, F.; Cuccia, L. A.; Capobianco, J. A. *J. Am. Chem. Soc.* **2006**, *128*, 7444.
(6) Pandozzi, F.; Vetrone, F.; Boyer, J. C.; Naccache, R.; Capobianco, J. A.; Speghini, A.; Bettinelli, M. *J. Phys. Chem. B.* **2005**, *109*, 17400.
(7) Rapaport, A.; Milliez, J.; Szipocs, F.; Bass, M.; Cassanho, A.; Jenssen, H. *Appl. Opt.* **2004**, *43*, 6477.
(8) Sivakumar, S.; Diamente, P. R.; van Veggel, F. C. J. M. *Chem.—Eur. J.* **2006**, *12*, 5878.

(9) Auzel, F.; Pecile, D. *J. Lumin.* **1976**, *11*, 321.
(10) Suyver, J. F.; Aebischer, A.; Biner, D.; Gerner, P.; Grimm, J.; Heer, S.; Kramer, K. W.; Reinhard, C.; Güdel, H. U. *Opt. Mater.* **2005**, *27*, 1111.
(11) Sivakumar, S.; van Veggel, F. C. J. M.; May, P. S. *J. Am. Chem. Soc.* **2007**, *129*, 620.
(12) Aebischer, A.; Heer, S.; Biner, D.; Kramer, K.; Haase, M.; Güdel, H. U. *Chem. Phys. Lett.* **2005**, *407*, 124.
(13) Bril, A.; Sommerdijk, J. L.; De Jager, A. W. *J. Electrochem. Soc.* **1975**, *122*, 660.
(14) Capobianco, J. A.; Vetrone, F.; Boyer, J. C.; Speghini, A.; Bettinelli, M. *J. Phys. Chem. B.* **2002**, *106*, 1181.
(15) Dong, B.; Song, H. W.; Yu, H. Q.; Zhang, H.; Qin, R. F.; Bai, X.; Pan, G. H.; Lu, S. Z.; Wang, F.; Fan, L. B.; Dai, Q. L. *J. Phys. Chem. C.* **2008**, *112*, 1435.
(16) Heer, S.; Kompe, K.; Güdel, H. U.; Haase, M. *Adv. Mater.* **2004**, *16*, 2102.
(17) Li, Z.; Zhang, Y. *Nanotechnology* **2008**, *19*, 345606/1.
(18) Li, Z. Q.; Zhang, Y. *Angew. Chem.* **2006**, *45*, 7732.
(19) Mai, H. X.; Zhang, Y. W.; Sun, L. D.; Yan, C. H. *J. Phys. Chem. C.* **2007**, *111*, 13721.
(20) Vetrone, F.; Boyer, J. C.; Capobianco, J. A.; Speghini, A.; Bettinelli, M. *J. Appl. Phys.* **2004**, *96*, 661.
(21) Wei, Y.; Lu, F. Q.; Zhang, X. R.; Chen, D. P. *Mater. Lett.* **2007**, *61*, 1337.
(22) Yi, G. S.; Chow, G. M. *Adv. Funct. Mater.* **2006**, *16*, 2324.
(23) Chatteriee, D. K.; Rufalhah, A. J.; Zhang, Y. *Biomaterials* **2008**, *29*, 937.
(24) Das, G. K.; Tan, T. T.; Y, *J. Phys. Chem. C.* **2008**, *112*, 11211.
(25) Diamente, P. R.; Burke, R. D.; van Veggel, F. C. J. M. *Langmuir* **2006**, *22*, 1782.
(26) Downing, E.; Hesselink, L.; Ralston, J.; Macfarlane, R. *Science* **1996**, *273*, 1185.
(27) Jalil, R. A.; Zhang, Y. *Biomaterials* **2008**, *29*, 4122.
(28) Mahalingam, V.; Mangiarini, F.; Vetrone, F.; Venkatramu, V.; Bettinelli, M.; Speghini, A.; Capobianco, J. A. *J. Phys. Chem. C.* **2008**, *112*, 17745.
(29) Schäfer, H.; Ptacek, P.; Zerzouf, O.; Haase, M. *Adv. Funct. Mater.* **2008**, *18*, 2913.
(30) Sivakumar, S.; van Veggel, F. C. J. M.; Raudsepp, M. *J. Am. Chem. Soc.* **2005**, *127*, 12464.
(31) Zhao, J.; Sun, Y.; Kong, X.; Tian, L.; Wang, Y.; Tu, L.; Zhao, J.; Zhang, H. *J. Phys. Chem. B.* **2008**, *112*, 15666.
(32) Li, Y. H.; Hong, G. Y.; Zhang, Y. M.; Yu, Y. M. *J. Alloys Compd.* **2008**, *456*, 247.
(33) Boyer, J. C.; Vetrone, F.; Capobianco, J. A.; Speghini, A.; Bettinelli, M. *J. Appl. Phys.* **2003**, *93*, 9460.
(34) Boyer, J. C.; Vetrone, F.; Capobianco, J. A.; Speghini, A.; Bettinelli, M. *Chem. Phys. Lett.* **2004**, *390*, 403.
(35) Boyer, J. C.; Vetrone, F.; Capobianco, J. A.; Speghini, A.; Zambelli, M.; Bettinelli, M. *J. Lumin.* **2004**, *106*, 263.
(36) Naccache, R.; Vetrone, F.; Mahalingam, V.; Cuccia, L. A.; Capobianco, J. A. *Chem. Mater.* **2009**, *21*, 717.
(37) Yi, G. S.; Chow, G. M. *J. Mater. Chem.* **2005**, *15*, 4460.
(38) Lisiecki, R.; Dominiak-Dzik, G.; Ryba-Romanowski, W.; Lukasiewicz, T. *J. Appl. Phys.* **2004**, *96*, 6323.
(39) Sangeetha, N. M.; van Veggel, F. C. J. M. *J. Phys. Chem. C.* **2009**, *113*, 14702.
(40) Kumar, G. A.; Chen, C. W.; Ballato, J.; Riman, R. E. *Chem. Mater.* **2007**, *19*, 1523.
(41) Bahtat, A.; deLucas, M. C. M.; Jacquier, B.; Varrel, B.; Bouazaoui, M.; Mugnier, J. *Opt. Mater.* **1997**, *7*, 173.
(42) Xiang, Q.; Zhou, Y.; Ooi, B. S.; Lam, Y. L.; Chan, Y. C.; Kam, C. H. *Thin Solid Films* **2000**, *370*, 243.
(43) Zampedri, L.; Ferrari, M.; Armellini, C.; Visintainer, F.; Tosello, C.; Ronchin, S.; Rolli, R.; Montagna, M.; Chiasera, A.; Pelli, S.; Righini, G. C.; Monteil, A.; Duverger, C.; Goncalves, R. R. *J. Sol-Gel. Sci. Technol.* **2003**, *26*, 1033.
(44) Sudarsan, V.; Sivakumar, S.; van Veggel, F. C. J. M.; Raudsepp, M. *Chem. Mater.* **2005**, *17*, 4736.
(45) Dong, C.; Raudsepp, M.; van Veggel, F. C. J. M. *J. Phys. Chem. C.* **2009**, *113*, 472.
(46) Sudarsan, V.; van Veggel, F. C. J. M.; Herring, R. A.; Raudsepp, M. *J. Mater. Chem.* **2005**, *15*, 1332.
(47) Liang, D. T.; Readey, D. W. *J. Am. Ceram. Soc.* **1987**, *70*, 570.

AM900630C